46th AIAA/ASME/SAE/ASEE Joint Propulsion Conference & Exhibit
25 - 28 July 2010, Nashville, TN

AIAA 2010-7114

Performance Evaluation of the T6 Ion Engine

John Steven Snyder,[*] Dan M. Goebel,[†] Richard R. Hofer,[*] and James E. Polk[‡]
Jet Propulsion Laboratory, California Institute of Technology, Pasadena, CA, 91109

Neil C. Wallace[§] and Huw Simpson[**]
QinetiQ Space Division, Farnborough, Hampshire, United Kingdom

The T6 ion engine is a 22-cm diameter, 4.5-kW Kaufman-type ion thruster produced by QinetiQ, Ltd., and is baselined for the European Space Agency BepiColombo mission to Mercury and is being qualified under ESA sponsorship for the extended range AlphaBus communications satellite platform. The heritage of the T6 includes the T5 ion thruster now successfully operating on the ESA GOCE spacecraft. As a part of the T6 development program, an engineering model thruster was subjected to a suite of performance tests and plume diagnostics at the Jet Propulsion Laboratory. The engine was mounted on a thrust stand and operated over its nominal throttle range of 2.5 to 4.5 kW. In addition to the typical electrical and flow measurements, an E×B mass analyzer, scanning Faraday probe, thrust vector probe, and several near-field probes were utilized. Thrust, beam divergence, double ion content, and thrust vector movement were all measured at four separate throttle points. The engine performance agreed well with published data on this thruster. At full power the T6 produced 143 mN of thrust at a specific impulse of 4120 seconds and an efficiency of 64%; optimization of the neutralizer for lower flow rates increased the specific impulse to 4300 seconds and the efficiency to nearly 66%. Measured beam divergence was less than, and double ion content was greater than, the ring-cusp-design NSTAR thruster that has flown on NASA missions. The measured thrust vector offset depended slightly on throttle level and was found to increase with time as the thruster approached thermal equilibrium.

I. Introduction

The Jet Propulsion Laboratory (JPL) has an ongoing interest in assessing electric propulsion systems and components for use in future deep space scientific missions for NASA.[1,2,3,4] With the recent launch of the Dawn spacecraft and the successful operation of its NASA NSTAR ion propulsion system, new and challenging deep space missions that can use ion propulsion to advantage are being investigated. These missions have various propulsive requirements, but generally require thrusters that throttle from 0.5 up to 7 kW in power at a specific impulse (Isp) of 2000 to over 4000 seconds, and have life and throughput capabilities well in excess of the NSTAR ion engine. Locating or developing thrusters that can satisfy these requirements is of considerable importance for future missions. Of equal importance is identifying system components such as the power processing unit (PPU), xenon feed system, and gimbal, with both high reliability (i.e. low risk) and acceptable cost.

QinetiQ Space Division has recently successfully flown the 10-cm T5 ion thruster on the ESA GOCE mission,[5,6] and its 22-cm T6 thruster has been selected for the ESA BepiColombo mission and is being qualified under ESA sponsorship for the extended range AlphaBus communications satellites platform. The T6 Kaufman-type thruster[7,8,9,10] has demonstrated nominal throttling capability from 2.5 to over 4.5 kW and produces a thrust level of 75 to 145 mN at an Isp of up to 4300 sec. For deep space applications of interest to NASA, the throttle range would need to be extended and the life validated for extended thrust durations of up to five years. QinetiQ has provided a

[*] Senior Engineer, Electric Propulsion Group, Senior Member AIAA.
[†] Senior Research Scientist, Propulsion and Materials Engineering Section, Associate Fellow AIAA.
[‡] Principal Engineer, Propulsion and Materials Engineering Section, Associate Fellow AIAA.
[§] Electric Propulsion Chief Engineer.
[**] Senior Engineer, Electric Propulsion Team.

T6 thruster to JPL for testing and evaluation with respect to NASA missions, as well as to gather information necessary for the planned applications of the T6.

II. Test Setup and Methods

A. Test Article and Facility

The T6 ion thruster, shown schematically in Fig. 1, is a Kaufman-type thruster with two 22-cm diameter grids. A unique feature of Kaufman thrusters is that they utilize a baffle electrode to disperse the cathode plume and improve the plasma uniformity across the acceleration grids, but this usually requires operation at higher discharge voltages (e.g. 30 to 40 V) than other types of thrusters for good performance.[11] The T6 thruster has been optimized to run at a discharge voltage of about 30 V. A weak magnetic field is created by solenoids located on the periphery of the discharge chamber. The field strength is fine-tuned with an external power supply for discharge optimization over a wide range of operating conditions.

The grids are dished in a concave fashion which causes the beam to focus to a waist and then diverge as a typical thruster plume. The screen grid is fabricated from molybdenum while the accelerator grid is made from high-density graphite to increase engine lifetime. An additional design feature is that the screen grid apertures have varying diameters across the grid to compensate for plasma density profile variations inside the discharge chamber.[7]

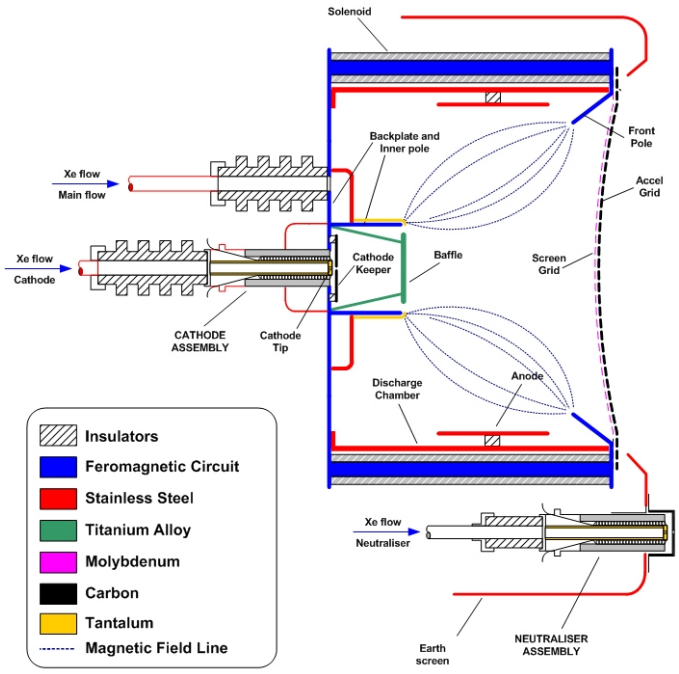

Fig. 1. T6 Thruster Schematic.

The engine includes an integral neutralizer mounted on the plasma ("earth") screen. Two additional neutralizers with slightly different geometries were also tested with the engine; further description may be found in Section IIIE.

All testing was performed in the JPL Patio Chamber facility. The vacuum chamber is 3 m in diameter and 8.6 m long, with ten cyropumps installed and operational for this testing. With the vacuum chamber configuration used for this test the effective pumping speed was approximately 160,000 L/s on xenon. To minimize facility backsputter rates the interior of the vacuum facility is lined with graphite panels. Electrical power and xenon flow were both provided with standard laboratory systems. Flow and electrical instrumentation were calibrated prior to testing.

The power system, flow system, and facility telemetry were controlled and monitored with a Labview-based data acquisition and control system. The data system recorded thruster currents, voltages, flow rates and temperatures, and facility pressure and temperatures at a user-specified rate, typically several times a minute. The software used to record data was also used to control thruster power supplies and flow rates. Xenon flow was controlled with a closed-loop controller; beam current was controlled in an open-loop fashion by manually adjusting the solenoid current at fixed discharge current and flow rates.

B. Diagnostics

1. Thrust Stand

Thrust measurements were acquired using the same water-cooled, inverted-pendulum thrust stand with inclination control and active damping that was used for the NSTAR Extended Life Test.[12] Calibrations were performed *in situ* by deploying a series of known weights spanning the range of 39 to 302 mN, ten times each. When inclination and thermal drift were accounted for during post-processing, the response of the thrust stand was repeatable and linear to the applied force. Thermal drifts of the thrust stand zero are typically the single largest uncertainty in the measurement. To minimize these effects, thrust stand data were collected only after the thruster had operated at a single condition for a minimum of two hours. Analysis of thrust stand data indicated a thrust

uncertainty of approximately ±1.5%. A photograph of the T6 engine operating at full power on the thrust stand is shown in Fig. 2.

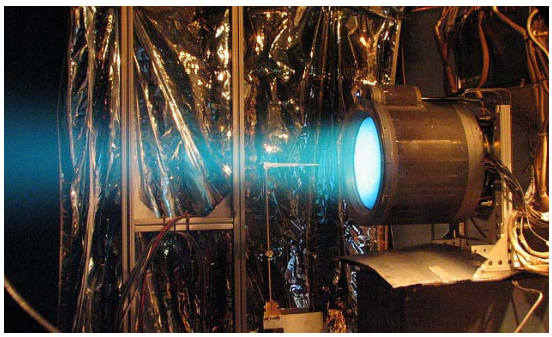

Fig. 2. T6 Operation at 4.5 kW During Thrust Measurement in JPL Facility.

2. Plasma Probes

An E×B probe and a Faraday probe were mounted on a three-axis positioning system to acquire plume data downstream of the engine. The probes could be moved axially and radially with respect to the thruster centerline as well as rotated about a line orthogonal to these axes. The disc-shaped Faraday probe was comprised of a 2.85-cm^2 graphite collector and a guard ring, both biased to -20 V for current density measurements. The E×B probe was used to determine the doubly-charged ion content in the plume. The probe, described in detail in Ref. 13, imaged a ~3-mm-dia. spot on the center of the grids when at its nominal axial location of 134 cm. For all data presented here, the probe was aligned with the local ion current density vector by rotating it such that the measured singly-charged ion current was maximized. Additionally, for measurements at the thruster centerline, the probe was positioned at the location of maximum ion current density as determined from the Faraday probe data. Off-centerline E×B probe data are referenced to this location. The doubly-to-singly-charged xenon ion current ratios presented here are those at the thruster exit plane, determined from the far-field measurements and calculated charge-exchange reaction rates using measured tank pressures. A review of error sources including probe alignment, current measurement, tank pressure measurement, and charge-exchange cross-sections indicated that uncertainty associated with the probe alignment dominated. Error bars shown along with the E×B data resulted from characterization of these effects during preliminary testing.

A suite of near-field probes were also mounted on a radial stage for measurements of plasma parameters 1 cm downstream of the front mask of the engine, across the face of the engine. A 0.5-mm-diameter, 1.65-mm-long cylindrical Langmuir probe was used for electron temperature measurements. A 3-mm-diameter flat-disk flux probe was used for ion current density measurements. Finally, an emissive probe constructed of 0.127-mm-diameter tungsten wire was used to measure local plasma potential.

3. Thrust Vector Probe

The T6 thrust vector was measured using a probe consisting of a square array of graphite rods at the far end of the vacuum chamber as shown in Fig. 3. Sixteen rods were positioned in the horizontal direction and sixteen in the vertical direction. The rods were 9.5 mm in diameter and 1.2 m long, with the rod centers located 7.0 cm apart. The front of the thrust vector probe was located 519 cm from the front mask of the engine. The rods were biased to -20 V to repel electrons, and the ion current collected by each rod was determined by measuring the voltage drop across a precision metal film resistor. Voltages were collected by the automated computer data acquisition system, and an end-to-end electrical calibration of the system was performed by driving currents through each of the rods. This system was used for thrust vector measurements in the NSTAR thruster program[14] but for the present test program the probe was refurbished including replacement of the graphite rods which had worn during the NSTAR Extended Life Test.

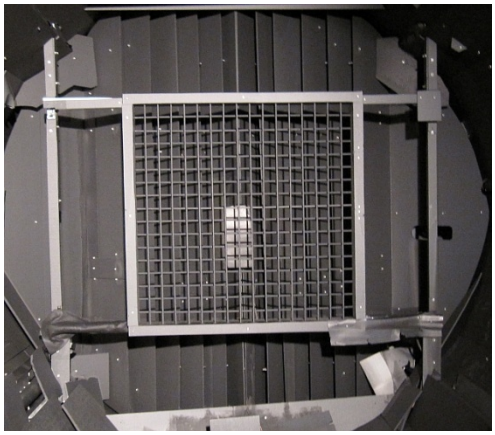

Fig. 3. Thrust Vector Probe, Located at Far End of Vacuum Chamber.

As described by Polk et al.,[14] use of the probe to measure the temporal thrust vector assumes that: the beam current density and thrust density distributions have a common centroid; the rod current is proportional to the beam current density integrated across the beam at the location of the rod; and all rods respond identically to impinging ions and the response varies uniformly over the entire probe with time. Under these conditions the currents measured by a set of rods can be used to approximate the location of the centroid in both the horizontal and vertical directions, and the intersection of the two centroids defines the intersection of the thrust vector with the probe.

A sample of data collected by the probe vertical rods during operation at the 125 mN operating condition is shown in Fig. 4. The data are well-described by a Gaussian function. The location

of the centroid in the horizontal direction (as measured by the vertically-oriented rods) determined from the fit was 433 ± 6 mm in the probe frame of reference. The intersection of the thruster geometric centerline with the thrust vector probe in the probe frame of reference was determined by direct measurement with a Leica TDM-5000 theodolite, which enabled direct calculation of thrust vector using the fit data. Fits were performed for both horizontal and vertical rod data for each set of data collected to determine the thrust vector centroid as a function of time. Data were collected typically several times a minute.

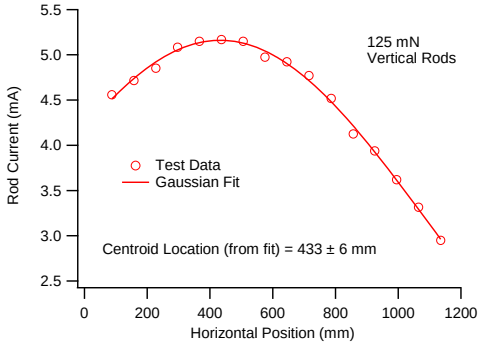

Fig. 4. Typical Thrust Vector Probe Data for a Single Time.

The uncertainty in the measured thrust vector was dominated by the uncertainty in centroid location determined from the curve fitting, which was typically in the range of 4 to 8 mm (i.e. less than the diameter of a graphite rod). Errors derived from current measurement, rod location measurement, and thruster centerline projection were all independent and significantly less than this. Hence, the maximum error in thrust vector due to uncertainty in inferring the centroid location from the rod currents was less than 0.1°.

Another possible source of uncertainty is due to the lack of knowledge of relative movement of the thrust stand, thrust stand mounting table, and thrust vector probe as the engine was fixed to the mounting plate on the thrust stand, and as the large vacuum chamber was evacuated, chilled by cryopumping, and warmed by thruster operation. The thrust vector probe and thrust stand mounting table were rigidly mounted to the vacuum tank and were not allowed to freely flex; the thrust stand was also rigidly mounted to the mounting table. The thrust stand itself is not a rigid structure although it is constrained to motion in the axial direction by design for sensing thrust. Active tilt control and sensing is employed as a normal part of thrust stand use, and the tilt was monitored during thruster mounting plate alignment measurement and actively controlled at the same position during thruster operation to limit pointing uncertainty associated with tilt (i.e. vertical motion of the thrust vector). Uncertainty in thrust vector measurement due to tilt control was less than 0.01°. Rotation in the yaw direction across the thrust stand mechanism (i.e. horizontal motion of the thrust vector) was limited by the design of the flexures and has not been quantified as a function of thruster installation or thermal stresses.

The total uncertainty in the vertical component of the thrust vector was thus about 0.1°. The total uncertainty in the horizontal component of the thrust vector was not quantified, but was at least 0.1°. Any additional uncertainty would be due to relative motion of facility equipment due to evacuation of the vacuum tank and heating and cooling of surfaces inside the tank. Since the equipment was all rigidly mounted and the thrust stand motion in that axis is constrained by design, significant additional uncertainty was judged to be unlikely.

C. Test Methods

Thruster performance and plume characterization were conducted at the four operating conditions shown in Table 1. Test conditions are referenced in this paper by their nominal thrust level. In contrast to ring-cusp engines such as NSTAR and NEXT, the discharge current of the Kaufman-type T6 is held constant and the beam current is adjusted by tuning of the solenoid current. As the engine warms the solenoid current must be continually adjusted to hold the beam current constant; this was done in open-loop control for the testing described herein. For example, at the 145 mN condition the solenoid current required to maintain the beam current set point was 1.2 A upon ignition of the cold engine, fell rapidly to 0.86 A within 8 minutes and then slowly decreased, reaching a value of 0.78 A after 2.5 hours of operation.

Initial testing of the engine was performed to collect baseline performance data and validate operational procedures and diagnostic methods. Most of the performance and probe data presented here were collected over a series of four days of subsequent testing, one at each of the four standard operating conditions in Table 1. These tests were geared to collect information as a function of time as the thruster warmed from a start at non-operating temperatures, which are typically in the range of -10 °C to -20 °C in this vacuum facility when exposed to the nearby liquid-nitrogen shrouds and cryosails. Thruster telemetry and thrust vector data were acquired continuously. Far-field probe data were acquired at approximately 15, 30, 60, 90, and 120 minutes after engine ignition. During those measurements the presence of the probes in the plume interrupted data collection by the thrust vector probe. Near-field probe data were collected at equilibrium conditions.

Table 1. T6 Engine Controlled Parameters.

	Nominal Throttle Level			
	75 mN	**100 mN**	**125 mN**	**145 mN**
Screen Voltage (V)	1850	1850	1850	1850
Beam Current (A)	1.10	1.47	1.84	2.14
Accelerator Voltage (V)	-265	-265	-265	-265
Discharge Current (A)	12.2	14.1	16.5	18.0
Neutralizer Keeper Current* (A)	1.0	1.0	1.0	1.0
Main Flow Rate (sccm)	10.6	16.0	21.2	25.8
Cathode Flow Rate (sccm)	7.0	7.0	7.0	7.0
Neutralizer Flow Rate* (sccm)	3.0	3.0	3.0	3.0

* Operating conditions for non-optimized neutralizer.

III. Test Results

Thruster performance, plume surveys, and thrust vector data were acquired for each of the four nominal throttle levels using the same procedure of thruster ignition from cold non-operating temperatures (-10 °C to -20 °C). In each case the non-optimized neutralizer that was packaged with the engine was utilized. Data from these tests are presented in the Sections A through D. Some of the E×B data were acquired in a prior series of baseline tests and those will be clearly identified in the discussion. The performance of the two additional neutralizers was characterized and is presented in Section E. Finally, performance calculations are given in Section F.

A. Thruster Performance

Measured, non-controlled thruster performance parameters acquired approximately two hours after engine ignition are summarized in Table 2. These values agreed extremely well with the data provided by the manufacturer. Measured thrust values matched the nominal thrusts within the measurement uncertainty. At the highest power level of 4.5 kW the T6 produced 143 mN of thrust at an Isp of 4120 seconds and 64% efficiency. Note that this performance data was acquired with a neutralizer flow rate higher than initially recommended by QinetiQ in order to keep the neutralizer out of plume mode. Subsequent measurements using an alternate neutralizer design provided by QinetiQ, to be discussed later, reduced this neutralizer flow requirement to 1.5 sccm and thus increased the specific impulse of the engine to over 4300 sec at the highest power point. Calculation for the discharge loss values includes the contribution of the solenoid power, which was only 2% of the discharge power at each test condition.

Table 2. Measured Engine Performance.

	Nominal Throttle Level			
	75 mN	**100 mN**	**125 mN**	**145 mN**
Beam Voltage (V)	1839	1838	1837	1836
Accelerator Current (mA)	7.2	8.7	11.1	15.7
Discharge Voltage (V)	30.90	30.05	30.42	29.89
Solenoid Current (A)	0.59	0.65	0.72	0.78
Solenoid Voltage (V)	10.7	12.2	14.0	15.7
Neutralizer Keeper Voltage* (V)	16.1	14.4	15.2	15.0
Floating (Coupling) Voltage (V)	-15.7	-15.2	-15.9	-16.0
Tank Pressure (Torr Xe)	1.6E-06	2.2E-06	2.5E-06	3.2E-06
Total Power (kW)	2.43	3.16	3.92	4.50
Discharge Loss (eV/ion)	346	292	276	256
Propellant Utilization*	0.697	0.725	0.742	0.753
Thrust (mN)	73.8	99.2	123.1	142.7
Specific Impulse (sec)*	3710	3940	4080	4120
Total Efficiency*	0.550	0.601	0.622	0.636

* Operating conditions for non-optimized neutralizer.

Operationally, the thruster was found to be very stable and easy to run. The recycle rate decreased from about once an hour during the first 5 to 10 hours of operation to once in 10 hours after a few days of running. The thruster also reliably cold started to full power operation in a matter of seconds. This is an advantageous feature of the concave grids used in the T6, where the more rapidly heated screen grid expands away from the accelerator grid during startup, in contrast to the convex grids of NSTAR that tend to close the gap and can even short during fast ramping to maximum power. No pre-heating period was required with the T6 thruster to achieve full power cold starts. Finally, the magnetic field of the Kaufman thruster produced by the solenoids provides a convenient mechanism to control the thrust level. Small changes in the solenoid current were used to regulate the thrust level at fixed discharge values as the thruster warmed during initial turn-on.

B. Ion Beam Profile and Divergence

The far-field Faraday probe was scanned radially across the beam at three axial locations from the thruster to determine the beam profile and angular divergence. Shown in Fig. 5 are the beam current densities measured at the maximum and minimum power levels as a function of axial and radial position. Note that the peak beam current density is not located on the thruster centerline; as will be shown later the engine thrust vector is offset from the geometric centerline and directed this way. Closer inspection shows that the peak moves toward more negative radial positions as the beam moves downstream.

Faraday probe data were used to characterize the engine beam divergence as a function of operating condition. In lieu of ascribing a divergence half-angle which has little engineering application, thrust loss factors are used here to characterize the beam divergence. They were calculated using the standard relationship:[11]

$$F_t = \frac{\int_0^r 2\pi r\, j_b(r) \cos\theta(r)\, dr}{\int_0^r 2\pi r j_b(r)\, dr} \qquad \text{Eq. 1}$$

where F_t is the thrust loss factor due to divergence, j_b is the beam current density measured by the Faraday probe, r is a radial position from the thruster centerline, and θ is the angle between the assumed point source of spherical expansion located on the thruster centerline and the radial position r. Two complications arise with implementing Eq. 1. First, the Faraday probe does not screen out non-beam ions (i.e. scattered or charge-exchange ions) at the beam wings, which means that the integration limits must be chosen carefully so as not to improperly weight the thrust loss factor by counting those ions. Second, spherical expansion is implicitly assumed. The expansion point source cannot be arbitrarily assigned to a location at the thruster without investigation of the beam behavior.

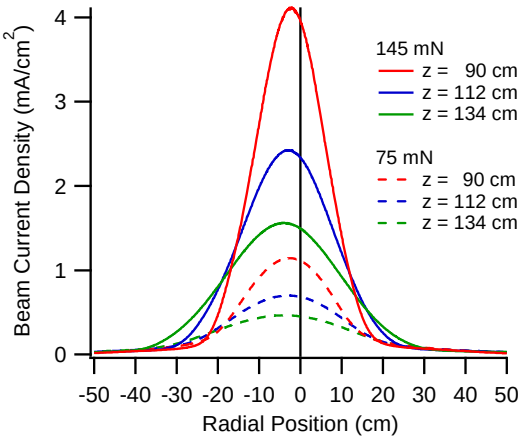

Fig. 5. T6 Beam Profile Data at Maximum and Minimum Power Operating Conditions.

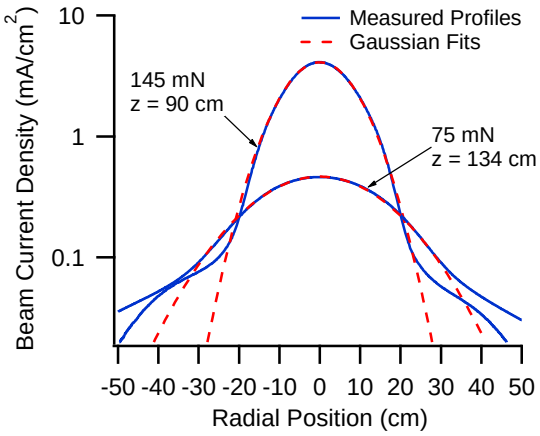

Fig. 6. Gaussian Fits to Beam Profile Data for Highest and Lowest Measured Peak Current Density Cases.

Integration limits were addressed by noting that the measured beam profiles are very well described by a Gaussian function over nearly the whole core of the beam for all operating conditions and axial locations, as shown in Fig. 6. Hence, it was assumed that a Gaussian fit to the beam profile represents the core beam current and excludes the incidental current that should not be counted as a contribution to the thrust loss factor. The beam profiles were also well-modeled by assuming spherical expansion from a point located 10 to 20 cm downstream of the engine, depending on the operating condition. This is much nearer to the thruster than is the geometric center defined by the radius of curvature of the spherically-shaped grids. For full-power operation, the point source location was found to be 18.2 cm downstream of the engine. Shown in Fig. 7 are data measured at an axial location of 134 cm compared to data measured at the

two nearer positions and extrapolated to 134 cm using a spherical expansion model from the point source location. Excellent agreement was observed for this and the other operating conditions.

A thrust loss factor was then calculated for each operating condition and axial location from the engine, using Eq. 1 while employing the Gaussian fits to each beam profile and the point source expansion location (necessary to define the angle θ). Results of the calculations are shown in Table 3 along with the point source location, where the thrust loss factors calculated at each axial position have been averaged together (there was almost no difference between them, the standard deviations were less than 0.03%). There is only a small change in losses observed with thruster operating condition, indicating that beam collimation is generally independent of power.

The T6 divergence is contrasted with that of the NSTAR engines utilized on the Dawn spacecraft. Across the throttle range shown here, the T6 engine loses 1.4% to 1.7% of its thrust due to beam divergence. Data from the Dawn FT1 thruster[15] show losses of 2.3% to 3.3% across the throttle range, nearly twice that of the T6. This is likely due largely to the larger radius of curvature of the T6 engine grids.

C. Double Ion Content

Double ion content in the beam was measured with the E×B probe located 134 cm from the thruster exit. Data acquired at the beam centerline during transient testing are shown in Fig. 8a. Doubly-charged ion current ratios at the two higher powers were observed to decrease with time. The magnitude of the decrease is larger than both the measurement uncertainty and an observed slight tank pressure increase during testing can account for, suggesting that the change occurred within the engine as it approached thermal equilibrium. No such measureable change is observed for the two lower powers.

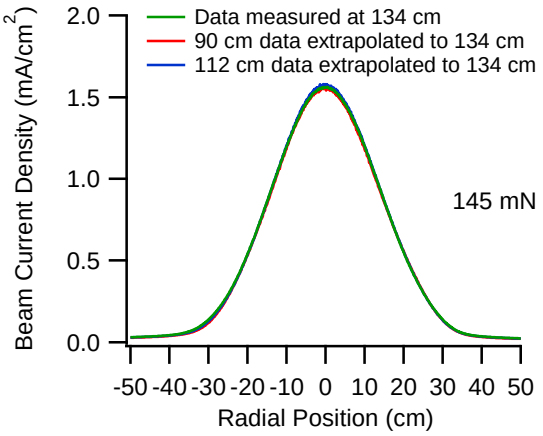

Fig. 7. Comparison of Measured Data with Spherical Expansion Model.

Table 3. Thrust Loss Factor due to Divergence.

Nominal Throttle Level	Apparent Point Source Location, z (cm)	Divergence Thrust Loss Factor, F_t
145 mN	18.2	0.986
125 mN	14.4	0.986
100 mN	13.2	0.986
75 mN	11.9	0.983

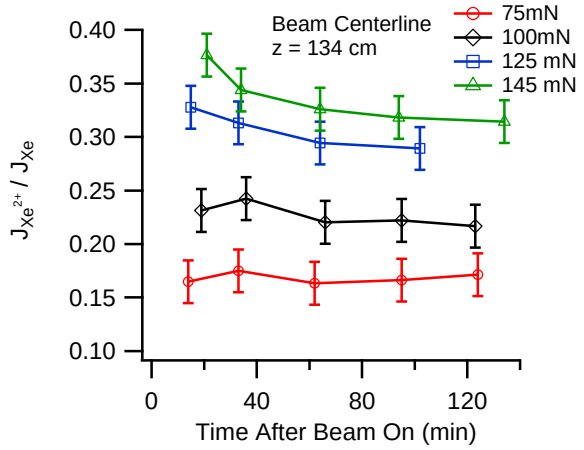

a) Temporal Variation on Centerline.

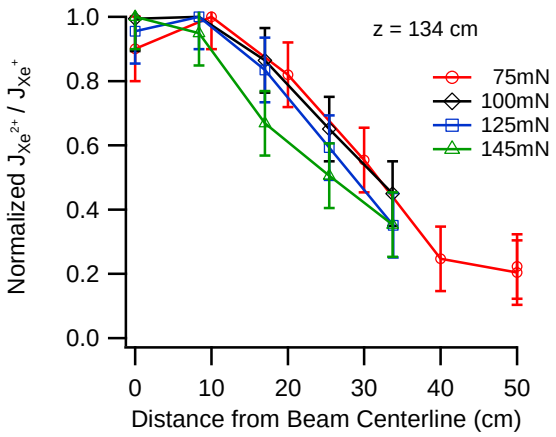

b) Normalized Radial Profile, After Two Hours of Operation.

Fig. 8. Doubly-Charged Ion Current Ratio Measurements.

Radial profile data were acquired by scanning the E×B probe in steps across the beam during the baseline testing, after the engine had been operating for at least two hours. The radial data, presented in Fig. 8b, were normalized by the steady-state values determined from Fig. 8a. The distribution is similar for all powers with a slightly lower concentration off-axis for the full power condition. A moderate amount of doubly-charged ions is visible outside the core of the beam. Global doubly-charged ratios were calculated by averaging the radial distributions of Fig. 8b with Eq. 2, and the results are shown in Table 4. This integration was performed using Gaussian fits to the beam current density data acquired at 134 cm downstream of the engine, and it is assumed that the results are representative of conditions at the thruster exit plane.

$$\frac{J_{++}}{J_{+}}_{avg} = \frac{\int_0^r 2\pi r\, j_b(r) \frac{J_{++}}{J_+}\, dr}{\int_0^r 2\pi r j_b(r)\, dr} \qquad \text{Eq. 2}$$

Table 4. Equilibrium Doubly-Charged Ion Ratios.

Nominal Throttle Level	Centerline Doubles Ratio	Engine-Averaged Doubles Ratio
145 mN	0.31	0.21
125 mN	0.29	0.23
100 mN	0.22	0.17
75 mN	0.17	0.13

Engine-averaged double ion content is higher than that of the NSTAR engines on Dawn, which range from ratios of 0.02 to 0.10,[15] largely because of the higher discharge voltage in the T6.

D. Thrust Vector

Thrust vector direction and migration was recorded at each of the four nominal throttle levels as a function of time using the probe at the far end of the vacuum chamber. Data are presented with respect to the coordinate system shown in Fig. 9, where the thruster exit plane is located in the x-y plane, the thrust vector is nominally pointed in the positive z-direction, and the x-axis is oriented in the 12 o'clock direction. In this system the thrust vector is defined by the spherical-coordinate angles ϕ (thrust vector orientation) and ω (thrust vector offset).

Thrust vector data collected at full power are shown in Fig. 10. Gaps in the test data exist where the far-field probes were collecting plume data. The thrust vector was initially offset from the thruster geometric axis by 2.2° and drifted to a 3.1° offset in steady-state operation. The orientation (i.e. clockwise motion) rose rapidly by 3º within three minutes of thruster ignition, then slowly fell to an equilibrium value of near 154° (i.e. approximately the 10 o'clock position when from viewed behind the engine). The trends in both angles follow exponential behavior with time, suggesting that thermal equilibration phenomena are important rather than abrupt mechanical or electrical changes within the engine. Time-dependent behavior in the spherical coordinate domain, depicting the net motion of the thrust vector in a spacecraft reference frame, is shown in Fig. 11.

Subsequent testing of the T6 at QinetiQ facilities indicated that the thrust vector deviation from the engine geometric centerline was caused by the particular grid set employed. Rotation of the grid set by 180º on the engine was observed to cause a 180º rotation of the thrust vector. Thrust vector migration was thus caused by relative thermal motion of the ion optics as they went from non-operating temperatures at the beginning of the test (-10 °C to -20 °C) to thermal equilibrium. Improvements in the thrust vector offset and migration are expected to be realized

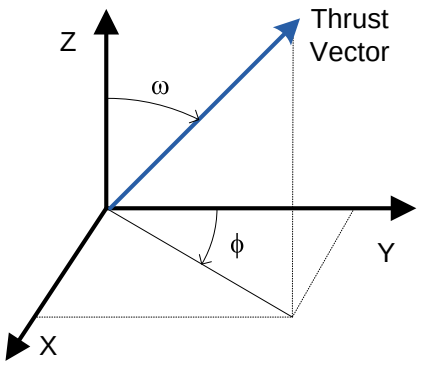

Fig. 9. Coordinate System for Thrust Vector Measurements.

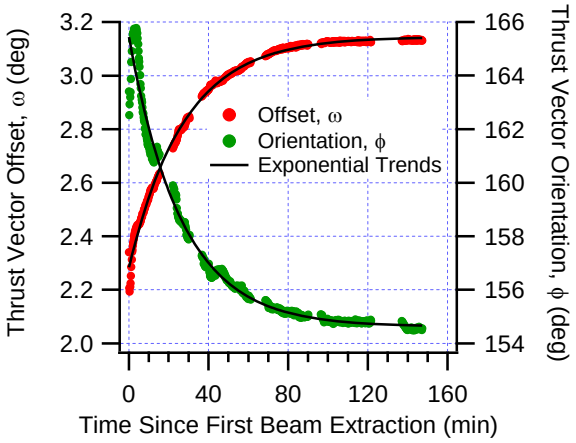

Fig. 10. Thrust Vector Migration at Full Power.

using improved assembly and grid alignment procedures developed by QinetiQ.

Migration data for all power levels are compared in Fig. 12. All thrust vector offsets are initially at the same value, as would be expected since the grids were at the same cold temperatures at the beginning of each test. There is a noticeable dependence on steady-state offset as a function of throttle level. Operation at higher powers should produce higher grid temperatures and thus more pronounced effects of relative thermal motion. A similar effect is seen for the thrust vector orientation where operation at lower powers produces a lesser change. Note that if the data for all four operating conditions were plotted on Fig. 11 in the spherical coordinate spacecraft frame of reference, the curves would nearly be coincident.

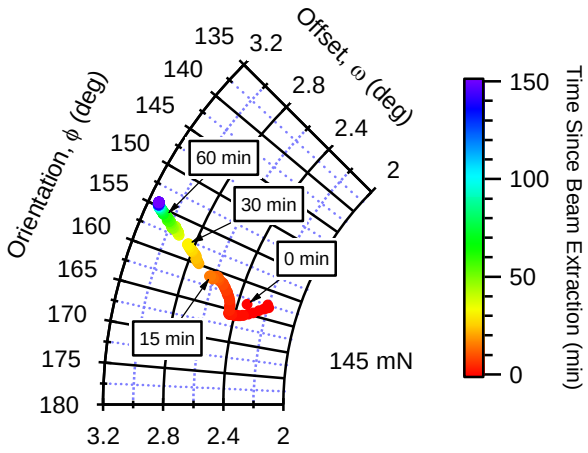

Fig. 11. Thrust Vector Migration at Full Power in Spherical Coordinate System.

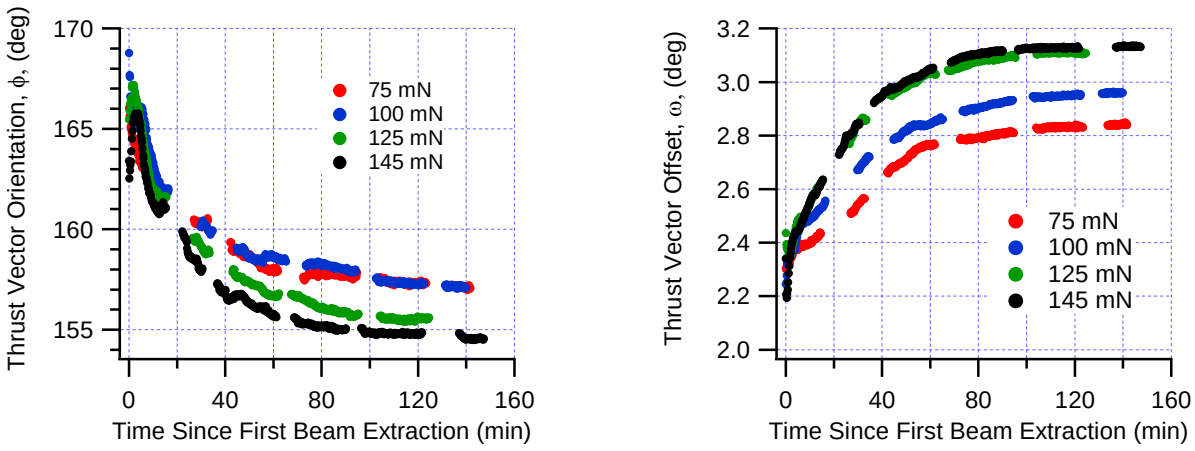

a) Thrust Vector Orientation. **b) Thrust Vector Offset.**

Fig. 12. Comparison of Thrust Vector Migration for Nominal Throttle Levels.

E. Neutralizer Characterization and Beam Plasma Measurements

The neutralizer originally packaged with the T6 thruster was specified to run at 1 sccm of xenon flow at a keeper current of 1.75 A. At these conditions and with the neutralizer common floating with respect to ground, measurements of the coupling voltage (i.e. neutralizer common to ground) and the keeper voltage oscillations indicated that the neutralizer was operating in plume mode.[16] This mode was nominally defined as a coupling voltage in excess of 20 V and a keeper voltage fluctuation level greater than 5 V peak-to-peak. The data shown in Table 2 were acquired with this neutralizer operating at 3 sccm of xenon flow, where the measured coupling voltage was near 15 V and the keeper voltage fluctuations less than 1 V_{pp}. While this took the neutralizer out of plume mode, the engine specific impulse was adversely affected by the higher flow rates used.

Operation in plume mode can lead to excessive neutralizer wear.[17] To address this issue, QinetiQ provided two additional neutralizers with smaller cathode orifice diameters for testing (62.5% and 50% of the original diameter). These were mounted next to the T6 and tested for plume mode onset during thruster operation. Shown in Fig. 13 are the coupling voltage and peak-to-peak keeper voltage fluctuations with the engine running at full power as a function of neutralizer flow rate and keeper current (J_{nk}) for alternate neutralizer #1. Operation at keeper currents in excess of 2.5 A is required to push the neutralizer out of plume mode at flow rates as low as 2 sccm. Increasing the keeper current to 4 A permitted operation at a flow of 1 sccm without plume mode onset.

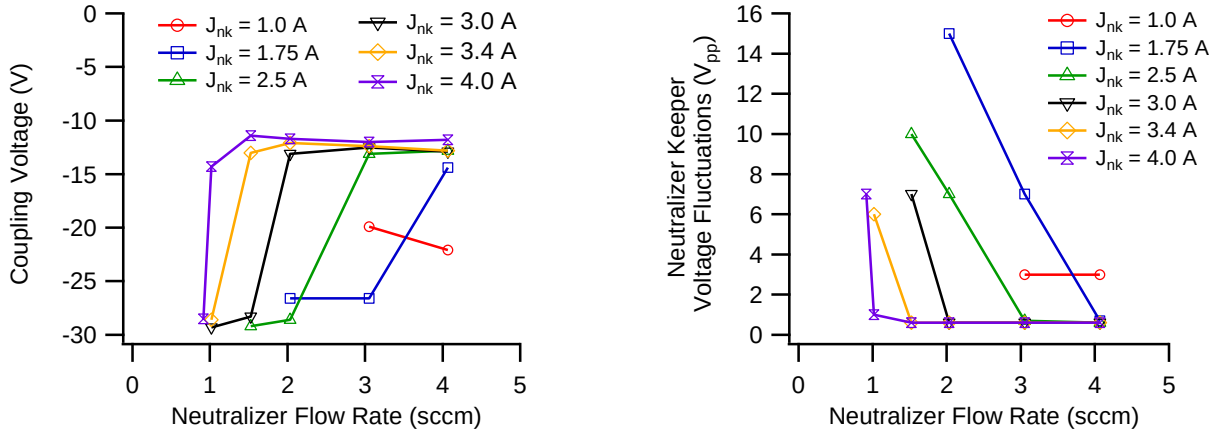

a) Coupling Voltage. **b) Neutralizer Keeper Voltage Fluctuations.**

Fig. 13. Alternate Neutralizer #1 Performance with Engine Operation at Full Power.

The plume mode margin for this neutralizer was determined by using the near-field probes to measure the local plasma potential and electron temperature. These plasma parameters are much more sensitive indicators of plume mode onset than keeper voltage oscillations,[16,17] which can be damped by the external keeper power supply circuit. The near-field data are shown in Fig. 14 as a function of neutralizer flow rate at a keeper current of 4.0 A. These data were acquired on the thruster centerline when the engine was operating at full power. Electron temperatures in the center of the beam were about 4 eV over most of the flow range, and only increased significantly at very low neutralizer flows near 1.0 sccm. The temperature at the edge of the beam (not shown) was found to be 0.5 to 1.0 eV lower than at the center. Plume mode onset developed near 1.0 sccm, and the neutralizer was clearly in plume mode at 0.9 sccm. Based on these data, it was determined that operating this neutralizer at 1.5 sccm and 4 A would provide a combination of low flow rate and at least 0.5-sccm margin against plume mode onset.

The second neutralizer cathode provided by QinetiQ had a smaller orifice than the one just described, but included a chamfer on the downstream side. This did not perform as well as the first neutralizer, it required more cathode flow and keeper current to avoid plume mode. Shown in Fig. 15 are plasma potential profiles relative to the neutralizer common potential across the front of the thruster for several neutralizer flow rates. These data were acquired 1 cm downstream from the front mask using a scanning emissive probe for the case of high power thruster operation (145 mN thrust) with 4 A of neutralizer keeper current. As the neutralizer flow decreases, the plasma potential increases substantially in spite of the fact that the neutralizer keeper voltage fluctuation level remained below 1 V_{pp} until the flow was reduced below 1.5 sccm. This behavior is indicative of plume mode onset at flow

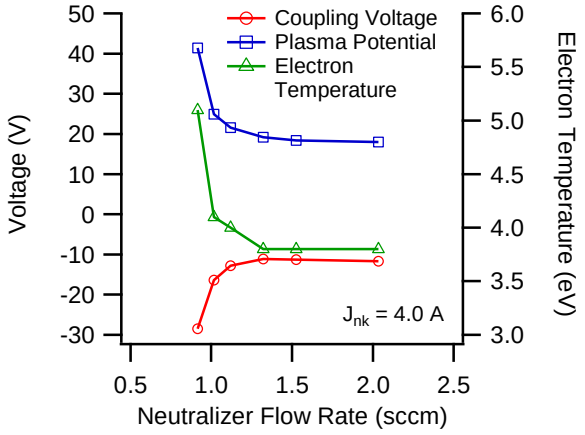

Fig. 14. Near-Field Plasma Characterization with Alternate Neutralizer #1 at Full Power (voltages are referenced to ground potential).

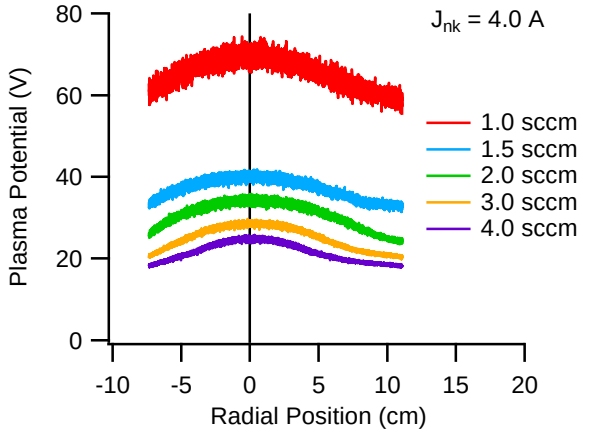

Fig. 15. Plasma Potential Profiles Relative to Neutralizer Common Near the Thruster Exit Plane for Alternate Neutralizer #2 at Full Power.

levels higher than 2 sccm. In this case, significant increases in plasma potential were observed when the flow was reduced below 3 sccm, compared to 1.5 sccm for the larger orifice cathode.

It is interesting to note that the plasma potential in the beam is at least 20 V positive relative to neutralizer common. This is the potential required to extract the required current from the neutralizer, and it increases with reductions in flow in the same manner as observed in discharge cathode behavior. Plume mode onset is more sudden as the flow is decreased compared to discharge cathodes, probably due to the reduced electron current emitted from the cathode orifice limiting the amount of ionization possible in the near-cathode plume. Since plume modes have been related to ionization instabilities in the near-cathode plume,[18] increases in plasma potential are expected as the discharge attempts to generate sufficient plasma to carry the current from the neutralizer to the beam.

F. Performance Calculation

Thruster electrical data, plume divergence, doubly-charged ion content, and thrust vector offset measured during the test campaign were used to calculate engine thrust according to:

$$T = \alpha F_t F_v \sqrt{\frac{2m}{e}} J_B \sqrt{V_B} \qquad \text{Eq. 3}$$

where the correction factor due to doubly-charged ions is:

$$\alpha = \frac{1+\frac{1}{\sqrt{2}}\frac{J_{++}}{J_+}}{1+\frac{J_{++}}{J_+}} \qquad \text{Eq. 4}$$

Note that an additional factor, F_v, has been added to the thrust equation (Eq. 3) which accounts for the measured thrust vector offset (the thrust loss due to divergence, F_t, was calculated only with respect to the beam centerline, not the engine centerline):

$$F_v = \cos\omega \qquad \text{Eq. 5}$$

Electrical data from Table 2, thrust divergence factors from Table 3, engine-averaged doubles ratios from Table 4, and thrust vector offsets from Fig. 12 were used to calculate engine thrust and are compared to the measured thrust in Table 5. Note that there is little change in thrust losses due to beam divergence and thrust vector offset as a function of power. The thrust losses due to doubly-charged ions are much greater, and also show a greater variation with power, than do the beam losses.

Lastly, engine performance was calculated for the optimized neutralizer operating parameters, i.e. a neutralizer flow rate of 1.5 sccm and a keeper current of 4.0 A as determined in Section IIIE, instead of the values used for the bulk of the testing. Here it is assumed that thrust losses due to doubly-charged ions, beam divergence, and thrust vector offset are unaffected by slight changes in neutralizer geometry and operating conditions. The results are shown in Table 6. In this configuration at full power the T6 will produce 143 mN of thrust at a specific impulse of 4300 sec and an efficiency of nearly 66%.

Table 5. Thrust Calculation Parameters.

	Nominal Thrust Level			
	75 mN	**100 mN**	**125 mN**	**145 mN**
α	0.966	0.957	0.946	0.949
F_t	0.983	0.986	0.986	0.986
F_v	0.999	0.999	0.999	0.999
Calculated Thrust (mN)	74.0	98.3	121.8	141.5
Measured Thrust (mN)	73.8 ± 1.1	99.2 ± 1.5	123.1 ± 1.8	142.7 ± 2.1

Table 6. Calculated Performance with Optimized Neutralizer.

	Nominal Thrust Level			
	75 mN	**100 mN**	**125 mN**	**145 mN**
Thrust (mN)	73.8	99.2	123.1	142.7
Specific Impulse (sec)	4000	4180	4290	4300
Total Efficiency	0.581	0.630	0.647	0.657

IV. Conclusion

The performance and plume characteristics of an engineering model T6 ion engine were evaluated at JPL. The engine performance was found to be very close to the values provided by QinetiQ at the four nominal throttle levels that were tested. The engine is characterized by its high specific impulse, which exceeds 4200 seconds at the highest power level. The total thruster efficiency is also significantly higher than the NSTAR thruster, which is largely due to the higher beam voltage of the T6 that offsets the higher discharge loss compared to NSTAR in the efficiency calculation. Issues with neutralizer operation in plume mode were handled by introducing a new neutralizer with a smaller cathode orifice and by modifying the flow and keeper current set points. At 4.5 kW the engine with the new neutralizer produced 143 mN of thrust at a specific impulse of 4300 seconds and a total efficiency of nearly 66%.

Beam current density profiles were used to calculate divergence thrust loss factors that were better than for the NSTAR engine, and that showed little if any dependence on engine power level. In contrast, doubly-charged ion ratios were higher than for NSTAR due to the higher discharge voltage. The doubly-charged ion content was observed to vary with time from engine startup and as a function of power level. A slight dependence on radial variation was also observed as a function of power level. The thrust vector showed a slight dependence on power and was offset from the engine geometric centerline, near 2º at engine ignition and slowly moving to near 3° at thermal equilibrium. Subsequent testing at QinetiQ, however, indicated this offset was attributable to the ion optics and is expected to improve with the implementation of better assembly and grid alignment techniques. Thrust magnitude calculated using the electrical telemetry and beam diagnostics matched the measured thrust within the measurement uncertainty.

Acknowledgments

The work described in this paper was carried out by the Jet Propulsion Laboratory, California Institute of Technology, under a contract with the National Aeronautics and Space Administration. Funding was provided by the QinetiQ, Inc. Special thanks go to Ray Swindlehurst and Allison Owens who were instrumental in setup and operation of the testing described herein.

References

[1] R.R. Hofer, T.M. Randolph, D.Y. Oh, J.S. Snyder, and K.H. de Grys, "Evaluation of a 4.5 kW Commercial Hall Thruster System for NASA Science Missions," AIAA 2006-4469, 42nd Joint Propulsion Conference, Sacramento, CA, July 2006.

[2] D.M. Goebel, J.E. Polk, R. Wirz, J.S. Snyder, I.G. Mikellides, I. Katz, and J.R. Anderson, "Qualification of Commercial XIPS Ion Thrusters for NASA Deep Space Missions," AIAA 2008-4914, 44th Joint Propulsion Conference, Hartford, CT, July 2008.

[3] J.S. Snyder, J.R. Anderson, J.L. Van Noord, and G.C. Soulas, "Environmental Testing of NASA's Evolutionary Xenon Thruster Prototype Model 1 Reworked Ion Engine," *J. of Propulsion and Power*, vol. 25, no.1, pps. 94-104, Jan.-Feb. 2009.

[4] J.S. Snyder, T.M. Randolph, R.R. Hofer, and D.M. Goebel, "Simplified Ion Thruster Xenon Feed System for NASA Science Missions," IEPC 2009-064, 31st International Electric Propulsion Conference, Ann Arbor, MI, Sept. 2009.

[5] N.C. Wallace, C. Saunders, and M. Fehringer, "The In-Orbit Performance and Status of the GOCE Ion Propulsion Assembly (IPA)," presented at the Space Propulsion 2010 Conference, San Sebastion, Spain, May 3-6, 2010.

[6] N.C. Wallace and M. Fehringer, "The ESA GOCE Mission and the T5 Ion Propulsion Assembly," IEPC 2009-269, 31st International Electric Propulsion Conference, Ann Arbor, MI, Sept. 2009.

[7] N.C. Wallace and M. Corbett, "Optimisation and Assessment of the Total Impulse Capability of the T6 Ion Thruster," IEPC 2007-231, 30th International Electric Propulsion Conference, Florence, Italy, Sept. 2007.

[8] N.C. Wallace, D.H. Mundy, D.G. Fearn, and C.H. Edwards, "Evaluation of the Performance of the T6 Ion Thruster," AIAA 1999-2442, 35th Joint Propulsion Conference, Los Angeles, CA, June 1999.

[9] J. Huddleson, J. Brandon-Cox, N. Wallace, and J. Palencia, "An Overview of the T6 Gridded Ion Propulsion System Pre-Development Activities for Alpha-Bus," SP-555, Proceedings of the 4th International Spacecraft Propulsion Conference, Cagliari, Sardinia, Italy, June 2004.

[10] N.C. Wallace, "Testing of the QinetiQ T6 Thruster in Support of the ESA BepiColombo Mercury Mission," SP-555, Proceedings of the 4th International Spacecraft Propulsion Conference, Cagliari, Sardinia, Italy, June 2004.

[11] D.M. Goebel and I. Katz, *Fundamentals of Electric Propulsion: Ion and Hall Thrusters*, Wiley and Sons, NJ, 2008.

[12] A. Sengupta, J.R. Anderson, J.R. Brophy, V.K. Rawlin, and J.S. Sovey, "Performance Characteristics of the Deep Space 1 Flight Spare Ion Thruster Long Duration Test after 21,300 Hours of Operation," AIAA 2002-3959, 38th Joint Propulsion Conference, Indianapolis, IN, July 2002.

[13] R. Shastry, R.R. Hofer, B.M. Reid, and A.D. Gallimore, "Method for analyzing ExB probe spectra from Hall thruster plumes," Review of Scientific Instruments, **80**, 063502 (2009).

[14] J.E. Polk, J.R. Anderson, and J.R. Brophy, "Behavior of the Thrust Vector in the NSTAR Ion Thruster," AIAA 1998-3940, 34th Joint Propulsion Conference, Cleveland, OH, July 1998.

[15] J.R. Brophy, C.E. Garner, and S. Mikes, "Dawn Ion Propulsion System – Initial Checkout after Launch," AIAA 2008-4917, 44th Joint Propulsion Conference, Hartford, CT, July 2008.

[16] D.M. Goebel, K.K. Jameson, I. Katz, and I. Mikellides, "Potential Fluctuations and Energetic Ion Production in Hollow Cathode Discharges," Physics of Plasmas, **14**, 103508 (2007).

[17] D.M. Goebel, I.G. Mikellides, J.E. Polk, J. Young, W.G. Tighe, and K. Chien, "Keeper Wear Mechanisms in the XIPS 25-cm Neutralizer Cathode Assembly," IEPC 2009-153, 31st International Electric Propulsion Conference, Ann Arbor, MI, Sept. 2009.

[18] D.M. Goebel, K.K Jameson, I. Katz, and I.G. Mikellides, "Plasma Potential Behavior and Plume Mode Transitions in Hollow Cathode Discharges," IEPC 2007-277, 30th International Electric Propulsion Conference, Florence, Italy, Sept. 17-20, 2007.